doi:10.1038/nature12760

Methods Summary

For inland waters we relied almost exclusively on calculated CO_2. CO_2 was calculated from pH, alkalinity and temperature using PhreeqC v2[51] or equilibrium constants reported by Stumm and Morgan (1996). Water chemistry data was culled from the literature and various governmental data sets and incorporated into the GLORICH database. Data were collected and digitized over a period of ten years. For this analysis, 6708 sampling locations were identified for streams and rivers and 25,699 single observations for lakes and reservoirs.

The surface area of inland waters was estimated using various geospatial products and scaling. For streams and rivers we utilized HydroSHEDS[24] and NHDplus to estimate length and hydraulic equations from the literature and USGS along with global gridded runoff data[27] to estimate width. This could only be done for regions <60^{o}N and for regions above this we utilized statistical relationships from regions <60^{o}N. For lakes and reservoirs we utilized the GLWD data set for lakes >3.16km^2 and utilized size distribution relationships from the literature [16,33] to extrapolate to smaller lake and reservoirs.

For streams and rivers we estimated the gas transfer velocity (k) using a recently published equation[30] that estimates k based on slope and velocity. Velocity was estimated using hydraulic equations from the literature and USGS along with global gridded runoff data[27]. Slope was determined using stream lines from HydroSHEDS and elevation from USGS Global Multi-resolution terrain elevation data[52]. For lakes and reservoirs we used two approaches for estimating the gas transfer velocity. The first utilized the relationship between *k* and wind speed given by Cole & Caraco (1998) while the second used the recently published relationship between lake area and *k* [21].

We calculated fluxes and tested the uncertainty of this efflux calculation using a Monte Carlo simulation (SI).

Stream and River CO_2

Water chemistry data was culled from the literature and various governmental data sets and incorporated into the GLORICH database[53]. Data were collected and digitized over a period of ten years. For this analysis 6708 sampling locations were identified to be applicable (Figure S1). In almost all cases pCO_2 was calculated from alkalinity, pH and temperature data. Calculation of CO_2 from alkalinity and pH can provide biased high values[9,54,55]. CO_2 cannot be calculated from alkalinity and pH at a pH less than 5.2 and provides erroneous results at pH slightly above 5.2. To minimize these biases we discarded all values with a pH <5.4. Further, erroneous pH values have a strong impact on calculated pCO_2 and produce unrealistic extreme pCO_2 values. To avoid the impact of such erroneous extreme values, we used median values per sampling location instead of means (means were approximately ~800µatm higher than medians). We further had to discard 8 sampling locations from a single study in South East Asia from the total of 6708 which had erroneous median pCO_2 values greater than 100,000µatm and were biasing interpolations.

For the spatial integration of stream/river pCO_2 data, and later for the spatially explicit calculation of stream/river-air CO_2 fluxes, we referred to COSCAT regions (a global segmentation scheme of coasts and the related river catchments[31]). To obtain a representative stream/river pCO_2 value for each COSCAT regions, we utilized all the calculated median pCO_2 values per sampling location (Figure S1) with the associated latitude/longitudes for a spatial interpolation in GIS. We applied an inverse distance weighted (IDW) approach that was structured to prevent interpolation across oceans and produced an interpolated grid at a 0.5x0.5 degree resolution. The gridded pCO_2 values were than averaged over the COSCAT regions. The spatial extent of the interpolation ended at the most northern and southern stations; all COSCATs, however, had at least one station within its borders and therefore were assigned a pCO_2 based on the values from the adjacent lower latitudes. Average COSCAT (see

below) pCO_2 was regressed against climate, land-cover and slope and none could explain a significant amount (r^2<0.1) amount of the variation.

In order to obtain a solubility coefficient (i.e., Henry's Law) to calculate dissolved CO_2 from the pCO_2 values, we estimated the average water temperature for each COSCAT from monthly climate data. For this, we established a relationship between water temperature and air temperature for each COSCAT that had more than 9 measurements of water temperature (from GLORICH) and an air temperature greater than -5^{o}C (water temp= air temp*0.67+7.45; r^2=0.65, p<0.001). To obtain a normalized global average CO_2 we simply weighted the CO_2 concentration of each COSCAT by the fraction of stream/river surface area (see next section) in that COSCAT:

$$Global\ CO2 = \frac{\int_{231}^{1} CO2i * SAi}{SAt} \quad (1)$$

Where CO2i and SAi are dissolved CO_2 and stream surface area from each individual COSCAT (of the 231 total) and SAt is the total stream surface area of the globe.

Stream and River Surface Area

The surface area of streams and rivers was determined by estimating the width and length of streams by stream order for each COSCAT region. We also estimated the percentage of ephemeral streams and the duration of ephemeral conditions for stream orders 1-5 (see below). The stream order length and basin area information from HydroSHEDS is not available for regions above 60^{o}N and for some small COSCAT regions and therefore we could only calculate stream surface areas for 193 of 231 COSCAT regions. For the remaining COSCAT regions we estimated stream surface areas from the relationships between climate and surface areas within the 193 regions with hydraulic information (equations below).

Length

Stream length by stream order was derived from the 15s resolution HydroSHEDS dataset[24]. As it has been demonstrated that small streams are not captured in HydroSHEDS[56], we performed a comparison between HydroSHEDS and the NHDplus (a finer 30m resolution

dataset) stream length for USGS Hydrologic Unit Codes (HUCS) 1-18 (Figure S2). When directly comparing the length of stream orders assigned in HydroSHEDS versus NHDplus we see that HydroSHEDS greatly underestimates length. This is because a HydroSHEDS stream order 1 is really a stream order 2 in the NHDplus dataset. When we compare the length of a stream order in HydroSHEDS to the next stream order in NHDplus, we get good agreement (Figure S2). That is, a stream order 1 in HydroSHEDS is comparable to stream order 2 in NHDplus. This comparison demonstrated that the HydroSHEDS stream order classification is missing at least 1 stream order. According to some studies[56], HydroSHEDS may be missing two stream orders. For this analysis we added one to each HydroSHEDS stream order and estimated the length of the true stream order 1. To estimate the length of stream order 1 we first determined the Horton ratio for stream length[57,58] for stream orders 1-4 in HydroSHEDS data set (which are assumed to be true stream orders 2-5) for each COSCAT region:

$$\frac{L_{so+1}}{L_{so}} = R_l \quad (2)$$

where SO is a stream order X, and R_l is the Horton ratio for stream length. The ratio was averaged and multiplied by the length of HydroSHEDS stream order 1, to get a length for true stream order 1. Across COSCAT's this ratio averaged 2.1$\pm$0.43. Length summaries for regions covered by HydroSHEDS are provided in Table S1.

We estimated stream width using hydraulic geometry scaling theory [26]. According to hydraulic geometry scaling the width (W), velocity (V) and depth (D) of a stream is related to discharge (Q) through power law functions

$W=aQ^b$ (3)

$D=cQ^d$ (4)

$V=eQ^f$ (5)

Where a, c and e are the hydraulic coefficients and b, d, and f are the hydraulic exponents [26,29]. Since Q=W*D*V, the exponents sum to one and the product of the coefficients is one. In order to use scaling law theory we therefore had to assign a discharge to each stream order within each COSCAT region. We had an average discharge for each COSCAT region from GLOBAL NEWS [59], which is taken from Fekete et al. (2002) and had to be converted to a discharge ($m^3 s^{-1}$) for each stream order within each COSCAT region. To do this, we first

converted the GLOBAL NEWS discharge for the entire COSCAT region to a yield (m yr^{-1}) and assumed this discharge was spatially constant for the entire COSCAT region and therefore could be used for each stream order. In order to determine a discharge (m^3 s^{-1}) for each stream order we then computed the average watershed area for each stream order since yield*area provides discharge in m^3 s^{-1}. Watershed area by stream order was estimated by Guth [60] from HydroSHEDS, which we gathered by COSCAT for this analysis. The watershed size ratio for HydroSHEDS watershed stream order 5:4 using this data was 4.0±1.3 and 3.9±1.6 for watersheds 6:5. That is, each increase in stream order produces a watershed that is ~4 times larger. We then computed a discharge for HydroSHED stream orders 4-6. Of the 193 COSCAT regions below 60°N, 201, 187, 144 had 4th, 5th, and 6th order watershed, respectively. Seven of these COSCAT regions had zero discharge so width could not be calculated for any stream order and surface area was assumed to be zero.

The width was calculated from discharge for stream orders 4-6 (NHDplus stream order 5-7) within each COSCAT using Equation 3. The hydraulic exponents (b) and coefficients (a) for width were established from two different data sets. The first from Raymond et al (2012) are from a compilation of stream gas tracer releases (ln width= 0.423lnQ+2.56). The second we created for this study using USGS gauging station rating curve data from 9811 stations (Figure S3). We believe Raymond et al. (2012) stream gas tracer releases over estimate width because they are generally done at low flow. Furthermore consistent with other authors [26] we believe the gauging stations under-estimate width due to the selection of gauging stations with distinct morphology (i.e., confined width).

Using these computed widths for stream orders 4-6 we established R_w, (the ratio of stream widths[61]):

$$\frac{W_{so+1}}{W_{so}} = R_w \qquad (6)$$

Where R_w is the ratio of stream widths and SO is stream order. We then calculated a ratio for width for stream orders 4:5 and 5:6 for each COSCAT with corresponding discharge and determined a grand average width ratio of 2.0±0.32 (i.e., a doubling of width with each increase in stream order) using the USGS hydraulic values and 1.8±0.29 using the Raymond et al.[29] hydraulic values. Since we had a discharge for 201 of the 202 COSCAT's for stream order

4, we used this calculated width along with R_w to estimate a width for all other stream orders within each COSCAT region. We did not find a correlation between the width ratio and temperature or precipitation.

We also corrected for the drying up of streams which can decrease the surface area. Many streams are "ephemeral" or "intermittent" and run dry for part of the year and will not take part in water-atmosphere gas exchange. Global estimates of the amount of ephemeral/intermittent streams are lacking. We utilized the U.S. NHDplus data to constrain how ephemeral streams impacts stream surface area. The NHDplus marks stream segments that are ephemeral/intermittent, which we gathered and collated by stream order and HUC (hydrologic unit code) and looked for correlations between the number of ephemeral streams segments and monthly climate and watershed attributes. Within a stream order, we found that the percentage of ephemeral/intermittent streams correlated well with temperature and precipitation (multiple linear regression; Table S2). We used these correlations to estimate the fraction of stream length that is ephemeral in each COSCAT. In approximately 25% of the COSCAT regions, these equations predicted greater than 100% stream length was ephemeral due to very low precipitation in these regions compared to the training data from the U.S. We capped the maximum percentage ephemeral at 90%. For the COSCAT's below 60^{o}N with length estimates we predict that 69, 56, 49, 42, and 34% of stream orders 1-5 are ephemeral, respectively (Table S2).

We utilized the USGS data set to determine the number of days that ephemeral streams are not flowing. We were able to locate 7150 USGS sites that had days were flow was recorded as zero. Of these 7150 sites 4971 had 3 years of complete flow data. We assigned each of these 4971 sites to a stream order and determined its average monthly climate using climate data from 1990-2010. Within a stream order, we found that the percentage of days a stream is not flowing correlated well with precipitation and the coefficient of variation of monthly precipitation (Table s3). We used these correlations to estimate the fraction of stream days that are ephemeral in each COSCAT. Similar to the above, we limited the maximum percentage of days ephemeral to 90%. By combining the percent number of streams that are ephemeral with the number of days they are ephemeral we can estimate the impact of stream drying on

the global stream surface area. We estimate that ~5.5, 3.6, 2.6, 2.0, and 1.4% of the total surface area of stream orders 1-5, respectively, in regions below 60^{o}N are ephemeral. Thus although stream drying is widespread in many regions of the globe, its overall impact on stream surface area (84,000km^{2}) is dampened by the fact that these regions have a lower overall predicted stream surface area.

Stream area was then determined for each COSCAT by summing the product of width, length and ephemeral proportion by stream order within each COSCAT. The surface area for COSCATs above 60^{o}N were estimated from multiple regressions of the COSCAT's below 60^{o}N (Figure S4). Using a multiple regression, we found significant relationships between the natural log of % stream surface area (with ephemeral surface area subtracted) and the natural log of precipitation and temperature for the COSCAT regions below 60^{o}N:

Raymond et al: $\ln (\% SA) = \ln P * 1.04 - 5.01e^{-2} * T - 7.08$, $r^2 = 0.81$, $p < 0.0001$, (7)

USGS $\ln (\% SA) = \ln P * 1.21 - 5.46e^{-2} * T - 8.72$, $r^2 = 0.79$, $p < 0.0001$, (8)

Where ln (%SA) is the natural log of the percentage of stream surface area, ln P is the natural log of precipitation in mm yr^{-1} and T is temperature in degrees C. Thus conceptually we argue that there is a global regulation of stream surface area by climate. We provide a figure of this result after averaging the Raymond et al. (2012) and USGS output in Figure S4. It is worth pointing out that if we use a spatially constant width for stream orders globally we find a negative correlation between stream area and precipitation.

We also adjusted surface area for stream freezing. In cases where temperatures are low streams can freeze. The exact impact of stream freezing on basin wide gas fluxes is not documented. We therefore assumed that at monthly average temperatures below -4^{o} C gas exchange is blocked due to ice. This resulted in an "effective" loss of about 87,000km^{2} of the global stream surface area. It is this final stream surface area that is used in the efflux calculation.

Stream and River Gas Exchange Coefficient

We utilized average basin slope and flow velocity of streams to determine the gas exchange coefficient by stream order for each COSCAT. Velocity was determined identically to width, using the hydraulic exponents and coefficients for velocity (Equation 5) provided in Raymond et al. (2012) and from the USGS gauging station (Figure S3). We determined the slope of stream lines for stream orders 2-4 using HydroSHEDS and elevation from USGS Global Multi-resolution terrain elevation data[52]. We determined the slope ratio for HydroSHED stream orders 2:3 and 3:4 and took a grand average of these values (1.6±0.86) to determine the channel slope for stream orders less than 2 and greater than 4. K_{600} was estimated using equation 5 from Table 2 in Raymond et al. (2012; k_{600}= SV*2841+2.02, where S=slope and V=velocity). In order to correct k_{600} to regional water temperatures, we used the established relationship between water temperature and air temperature (see above) to obtain a k_{actual} for each region. A single k_{actual} for each COSCAT was obtained by normalizing the k_{actual} of each stream order to the surface area of that order (similar to equation 1 above). Similar to surface area this could only be done for the 193 COSCAT regions with stream length data. For the remaining high latitude areas we estimated k_{actual} from a multi-regression between the 193 regions and precipitation:

Raymond et al.: K_{actual} (m d^{-1}) = P*3.9e^{-3} + 2.7 (r^2=0.46) (9)

USGS: K_{actual} (m d^{-1}) = P*4.0e^{-3} + 4.7 (r^2=0.29) (10)

For both velocity and width we averaged the output obtained from using the equations from Raymond et al. (2012) and the USGS gauging stations (Figure S4). The Raymond et al. (2012) set of equations tend to overestimate width and underestimate velocity of low order streams and underestimate widths of high order streams because the data set is primarily from small to medium sized systems during low flow which will bias measurements to a higher width in small systems. The USGS data set provided lower estimates of low to mid order streams and similar values to the Raymond et al. (2012) equation for high order streams because data from gauging stations have unique hydraulics with average shorter widths and higher velocities than representative stream sections. Therefore we believe the best current estimate from the

hydraulic equations is to average the two. To obtain an average global k we simply weighted the value of each COSCAT k by the fraction of stream surface area in that COSCAT. We reported the average k and surface area in Table S1.

Since width and velocity are not related to discharge linearly, there is the potential for a bias by calculating them from annual average discharge. We performed a sensitivity analysis to compare calculating velocity and width daily from daily discharge from 2 random sites in the USGS data set (02454660 and 09243800) versus calculating width and velocity from an annual average. In both cases using daily values produced higher annual average velocities and widths and therefore we conclude that this bias does not inflate values.

Stream and River Gas Exchange

We performed a Monte Carlo simulation to estimate CO_2 efflux and provide an error estimate. We did this by providing a range in all three of the factors whose product determines the CO_2 flux, the gas transfer velocity, surface area, and CO_2 concentration gradient and randomly selecting data 1000 times from these ranges in order to iteratively estimate the resulting CO_2 flux. As mentioned, for both the gas transfer velocity and surface area we argue that the USGS and Raymond et al. (2012) hydraulic equation reasonably bound these estimates and we therefore used these two equations to obtain a range. The mean of the gas transfer velocities normalized to the surface area of streams and rivers in each COSCAT was 6.3 and 5.0 using USGS and Raymond et al (2012) equations, respectively. The estimated ice free surface area was 423,000 and 649,000 using the USGS versus Raymond et al. (2012) equations. Spatially within COSCAT's the range of gas transfer velocities and surface area could be larger or smaller than this global average. The coefficient of variation (CV) for surface area for instance ranged from 1.1 to 5.0% for individual COSCAT's (compared to the global CV of 3.1).

For the concentration of CO_2 we provided a range of concentrations that was dependent on the density of sampling locations with CO_2 values within each COSCAT region. We also attempted to account for the possibility that calculated CO_2 values are biased high (see stream and river CO_2 section). For COSCAT regions with more than 0.1 station for every km^2 (n=7) we assumed the error in the CO_2 value was +/- 20%. For COSCAT regions with 0.01-0.05

(n=26), 0.005-0.01 (n=12), 0.005->0 (n=33) and zero (n=146) gauges every km^2 we assumed an error of 30, 40, 50, and 60%, respectively. Multiplying these errors by the interpolated CO_2 for each COSCAT provided a high and low estimate of CO_2 for each COSCAT. Based on the comparison of measured and estimated CO_2 values in Butman and Raymond (2011) that demonstrate the potential for overestimation of CO_2 from calculations, we then assumed that the high estimate was 80% of the value estimated using the above calculation.

The regional estimates had a large range of error with the standard deviation of individual COSCAT's ranging from 0.01-51 g m^{-2} land surface yr^{-1} (Figure 5S).

Lake and reservoir CO_2

The Glorich-database contained 25,699 single observations of lake pCO_2 mostly from recent meta-data analysis that were derived from national inventories of lakes in Sweden, Finland and the USA [19,42,43,62-65]. Data derived from under-ice samplings in northern temperate lakes were excluded from the analysis, as the ice cover prevents atmospheric exchange and causes CO_2 accumulation. Those observations were identified by having water temperature <4°C and sampling dates ranging from December to April. Thus, the final dataset contained 20,735 observations of lake pCO_2. Almost all pCO_2 data are based on calculation from pH, alkalinity and temperature, either using Phreeqc v2 or equilibrium constants reported by Stumm and Morgan (1996). Direct measurements of pCO_2 were rare (<1% of observations). Even if most data originates from northern temperate regions, the dataset covers all major climatic zones. Reservoirs typically show highly elevated pCO_2 during the initial 10-15 years after impoundment due to decomposition of flooded soils and biomass [37,38], while the pCO_2 of older reservoirs tends to be similar to natural lakes[66,67]. Here, we applied the lake pCO_2 data to both lakes and reservoirs. Note that the pCH_4 of reservoirs has been reported to be different

from that of natural lakes irrespective of reservoir age[38], but that CH_4 emission is small in terms of carbon units.

Distributions of lake pCO_2 showed that tropical lakes and saline lakes were distinct from freshwater lakes in non-tropical climates[43,62]. The distribution of mean pCO_2 was skewed towards higher values in all three groups, and we therefore used the median as a representative value instead of the mean. For the non-tropical freshwater lakes, we found that lake pCO_2 was negatively related to lake surface area, and positively related to DOC concentration. As generally >90% of the TOC in lakes is made up of DOC, we assumed that TOC concentration is equivalent to DOC concentration. In lakes with a high concentration of dissolved organic carbon (DOC), the presence of organic acids anions may contribute to alkalinity [68] and affect the calculation of pCO_2. However, even when accounting for this effect, a strong positive relationship between pCO_2 and DOC concentration was observed in low-alkalinity and high-DOC boreal lakes [19]. As the variability in pCO_2 at any given lake area or DOC concentration was substantial, we classified lake pCO_2 into bins of lake area and DOC concentration. Lake area was binned into five $\log_{10}$ classes (1-10, 10-100, 100-1000, 1000-10000, >10000 ha), and DOC concentration was binned into 12 classes at 2.5 mg L^{-1} steps (0-2.5, 2.5-5, … 27.5-30 mg L^{-1}). For non-tropical and saline lakes, median lake pCO_2 could be modelled from binned lake area and binned DOC concentration as follows:

$$\text{median pCO2} = 1232(\pm 93) + 29.09(\pm 4.05)*\text{DOC} - 188.5(\pm 26.3)*\log \text{LA};\ R^2=0.72;\ p<0.0001, \quad (11)$$

where DOC is the midpoint of the binned DOC concentration in mg L^{-1} (e.g. 1.25 is the midpoint DOC for the 0-2.5 mg L^{-1} bin) and log LA is the midpoint of the binned $\log_{10}$ of lake

surface area in ha (e.g. 1.5 is the midpoint of the 1-2 $\log_{10}$ lake area bin, i.e. lakes in the 10-100 ha range). Fig 6S shows that this model provides a good fit over the range of most frequently observed pCO_2 in freshwater lakes. We tried to incorporate the tropical lakes into this model by adding a temperature effect into the regression, but we were not able to construct a model that accommodates the lack of a temperature effect on pCO_2 in the non-tropical lakes as well as a significantly higher pCO_2 in the high-temperature tropical lakes. Hence, we used the above model (Eq. 11) to estimate median lake pCO_2 for each non-tropical exorheic COSCAT, using the binned lake and reservoir area, and the modelled DOC concentration from GLOBALNEWS at the river mouth [59]. This procedure assumes that river mouth DOC is indicative of average lake DOC in each COSCAT [69].

Because of the comparative data scarcity for tropical and saline lakes, we were not able to construct any models for pCO_2 for those lakes. Instead, we applied the median pCO_2 for tropical lakes (1906 µatm; this value excludes 4 extremely high outliers (>40000µatm) and 37 observations in Afro-alpine lakes) to all lakes in humid tropical COSCATs (identified by annual mean temperature >20°C and precipitation >1000 mm). For saline lakes, we used the median pCO_2 values of two calculation methods (freshwater and marine ionic composition scenario; see [43] for details), and calculated a mean of those (340 µatm), excluding 5 extremely high outliers (>35000 µatm). This value was applied to all lakes situated in endorheic COSCAT basins. This procedure neglects the presence of freshwater lakes in endorheic basins, but on the other hand disregards the occurrence of saline lakes in dry, exorheic basins. For the Caspian Sea, a saline lake and the largest inland water body on Earth, we used the median of reported pCO2 (690 µatm) instead[43].

Lake and Reservoir Area

The global lakes and wetlands database (GLWD) compiled by Lehner and Doll (2004) contains a virtually complete inventory of the world's largest lakes and reservoirs as well as incomplete data for lakes and reservoirs as small as 0.1 km^2. These data were truncated at $10^{0.5}$ km^2, or 3.16 km^2, in order to ensure completeness[16], and classified by COSCAT region[31].

The size distribution of lakes and reservoirs has been observed to follow the Pareto distribution[34], with the probability density function

$$pdf(a) = ck^c a^{-(c+1)} \qquad (12)$$

Where *a* is lake area, *c* is the shape parameter, and *k* is the minimum area. It has also been shown, however, that in the United States, a single parameterization of the Pareto distribution is insufficient to describe the size distribution of lakes and reservoirs across all size classes[16]. Thus, there is considerable uncertainty inherent in estimating global lake size and abundance based on the relatively few GLWD data. To incorporate this uncertainty, the 13 regional estimates of the Pareto shape parameter (*c*) presented by Downing et al. (2006) were combined with the 16 regional estimates of *c* presented by McDonald et al. (2012) to establish a median value of 0.79 (mean = 0.85, sd = 0.18). A nonparametric estimate of the 95% confidence interval about this value was made by calculating the 2.5th and 97.5th percentiles of the data set 0.62, and 1.25, respectively.

Because cumulative Paretian data is linear on a log-log scale, simple linear extrapolation was used to estimate the number and size of lakes below the resolution limit of the GLWD data. This analysis assigned the commonly chosen 0.001 km^2 as the minimum size of lakes and

reservoirs. While there are many water bodies throughout the world smaller than this, they contribute relatively little to the total surface area[16]. The cumulative number of lakes/reservoirs between A_{min} and A_{max} in each COSCAT region, *i*, was calculated as:

$$\log(cumulative\ abundance_i) = \log(upper\ intercept_i) + (\log(A_{max}) - \log(A_{min})) * c\ , \quad (13)$$

where *upper intercept* is equal to the number of GLWD lakes/reservoirs greater than A_{max} in region *i* plus one, and *c* is the Pareto shape parameter. Size classes used in this analysis were defined as shown in table S4, with the exception of 1-10 km^2, which was split into 1-$10^{0.5}$ km^2 (extrapolated) and $10^{0.5}$-10 km^2 (GLWD data).

The mean surface area of lakes/reservoirs in each size class was calculated following Equation 8 in Downing et al. (2006). This area was then multiplied by the extrapolated abundance of lakes in each size class in each COSCAT region to obtain total surface area. Equation 10 was applied using the median and 95% confidence limits for *c*. It was assumed that there is no error in the GLWD data, and confidence intervals were propagated throughout the calculation. Total lake areas by size class are shown in Table S4.

Lake and Reservoir Gas Exchange Coefficient

We used two alternative approaches to derive the gas exchange coefficient for lakes and reservoirs. First, we used wind speed averaged for each COSCAT and the relationship between k_{600} and wind speed given by Cole & Caraco [21]. Second, we used the recently published

relationship between lake area and k_{600} [22] to derive mean k_{600} for lake area bins (0.54, 1.16, 1.32 and 1.90 m d^{-1} for lakes <0.1, 0.1-1, 1-10 and >10 km^2, respectively). The wind speed relationship [21] is derived from whole-lake tracer addition experiments and is widely used for calculating CO_2 emission, but returns a low estimate of k_{600} compared to other studies [71-73] and will therefore result in conservative CO_2 emission estimates. Using the mean k_{600} for classes of lake area[22] incorporates the differential effects wind has on k_{600} depending on lake area, since large lakes are more wind-exposed and turbulent, thus exposing higher k_{600}, than small lakes. However, the k_{600} estimates by Read et al (2012) are derived from hydrodynamic calculations in the middle of the lake, where turbulence is frequently higher than in more sheltered bays, and may therefore overestimate whole-lake k_{600}. Therefore, the two approaches provide a low and a high estimate, and constitute a probable range of k_{600}. Temperature-adjusted *k* for each COSCAT was derived from the estimated k_{600} and annual mean temperature during ice-free months (monthly T>0°C), following Jähne et al. [74].

Lake and Reservoir Gas Exchange

The emission of CO_2 from lakes and reservoirs in each COSCAT was calculated for every size class bin by multiplying the air-water CO_2 concentration (assuming an atmospheric pCO_2 of 390 μatm) with the temperature-adjusted gas exchange coefficient *k* and the surface area of lakes and reservoirs. Based on reports of strong CO_2 accumulation under the ice cover of lakes, and very high emissions at ice-out, we did not discount the period of ice cover in emission calculations[75]. In this study, lakes and reservoirs were not analysed separately. However, given that our results indicate that tropical and large systems contribute disproportionally to CO_2

emission, the current increase in the number of large hydropower dams in the tropics implies that reservoirs will become increasingly important for overall CO_2 emission from inland waters, warranting for more detailed future studies.

Error Analysis

We performed a Monte Carlo simulation for every lake area class bin in every COSCAT in order to estimate the error in our estimates. This was achieved by randomly picking values from uncertainty intervals of pCO_2, area and k, and 1000 iterative calculations of the resulting CO_2 flux. The median of these 1000 fluxes was used as a statistically balanced estimate of CO_2 emission, and the 5^{th} and 95^{th} percentiles as measures of its uncertainty. For pCO_2 of the non-tropical freshwater lakes, we used the standard errors of the coefficients of the regression model (Equation 10) to calculate a range from which to randomly select values. The standard errors were used instead of the confidence intervals because using the latter resulted in unrealistic (e.g. negative) values of pCO_2. For tropical lakes, we used the interquartile range of the observed pCO_2 (680-4775 µatm) as uncertainty range. For saline lakes, we used the maximum extent of the interquartile ranges of the two ionic composition (freshwater and marine ionic composition scenario; see [43] for details) scenarios (81-1414 µatm). For the Caspian Sea, pCO_2 was randomly picked from the range of observed values (510-1120 µatm[43]) For lake and reservoir area, random values were selected from a lognormal distribution defined by the mean area and its 95% confidence interval. For the gas exchange coefficient *k*, random values were selected from the range of k provided by the two different estimates (Cole and Caraco

1998 or Read et al. 2012). Median CO_2 emission and its 5^{th} and 95^{th} percentiles were summed across lake area bins and COSCATs in order to calculate total CO_2 emission.

Since the first publication of CO_2 emission from global lakes, there has been a steady trend towards higher estimates by every new paper (Fig. S7). We calculated a lower CO_2 emission from lakes and reservoirs of ~0.32 Pg C yr^{-1} as compared to recent studies (Table S4), and estimated a large uncertainty interval (0.06-0.84 Pg C yr^{-1}).

Sensitivity Discussion

The large uncertainty level in lakes illustrates the gaps in basic understanding of processes at the global scale. For lakes, a large source of uncertainty is in the surface area calculations of small lakes. Any future change in the surface area will proportionally impact the global flux. It will also redistribute the relative importance of small versus large lakes, since large lakes are currently counted and their area will presumably not change greatly. Currently we discount the gas transfer velocity in small lakes based on only a small number of measurements and thus future research on the controls of k are needed and may change global fluxes. The annual flux of lakes, however, appears to be much smaller than streams and rivers.

We predict global hotspots of stream and river evasion. This is due to a high surface area and high gas transfer velocity in regions of the globe where precipitation is high. Unfortunately the data sets we currently use to model global stream and river hydraulics (width and velocity) are biased to temperate systems that generally have modest rainfall. We believe the general finding that regions that receive high precipitation have a higher surface area and gas transfer velocity is mechanistically defensible, but clearly more research is needed in these areas of the

globe. If we use our two set of hydraulic relationships separately to estimate global fluxes we obtain a difference of ~0.5 Pg yr^{-1}. In high latitude regions the situation is even worse, as current global maps of stream length are also lacking. The geomorphology of high latitude ecosystems (e.g., peatlands) and the extreme cold temperatures will probably lead to different scaling laws which need to be incorporated into future efforts. Currently we assume no fluxes in high latitude regions during months colder than -4^{o}C, which decreases global fluxes by 0.25Pg yr^{-1}.

The paucity of direct CO_2 measurements in inland waters is a major shortcoming. Unlike oceanic systems the chemistry of these waters is highly variable and lead to problems when calculating CO_2 from alkalinity and pH. Potential errors in historic pH measurements are also currently difficult to assess and adequately deal with. We tried here to overcome some of the potential biases by using medians for individual stations instead of means. We also did not assign higher CO_2 values to low order systems. Finally, we used a higher range in CO_2 for systems with fewer CO2 measurements and discounted the high values in our Monte Carlo by 20%. Although an average of 2,300 µatm for station medians and global spatially average pCO_2 of 3100 µatm are reasonable, the fluxes of Southeast Asia are particularly uncertain (Figure 5) and a region with very few but high CO_2 calculations (Figure 1). Since this region has high precipitation and therefore a high gas transfer velocity and surface area these high CO_2 values may be a source of overestimation. In our error analysis, when we assume that the variance of the CO_2 is 80% for the high CO_2 estimate for CO_2 for each COSCAT, the global stream and river flux decreases by ~0.35Pg yr^{-1}. If we utilize a CO_2 of 2300 µatm for each COSCAT, the global efflux falls by ~0.8Pg yr^{-1}.

Table S1. Global watershed stream attributes aggregated by stream order for regions <60°N. Active area is the area of stream surface area excluding ephemeral streams contributions but not including periods of ice over.

Stream Order	Ephemeral Stream Length km2	Total Stream Length km2	Active Area (km2)	kactual	% Flux
1	1.71E+07	2.48E+07	78177	10.4	25
2	6.67E+06	1.18E+07	75306	8.4	20
3	2.79E+06	5.62E+06	67688	6.8	14
4	1.16E+06	2.75E+06	62736	6.2	12
5	4.52E+05	1.32E+06	58361	5.2	9
6		6.39E+05	56304	4.5	8
7		2.69E+05	44940	4.0	6
8		8.78E+04	27773	3.6	3
9		3.71E+04	21670	3.2	2
10		4.17E+03	5308	3.0	0

Table S2. Statistics from ephemeral stream length estimation. All NHDplus stream length data was aggregated by HUC's 1-21. Presented are the coefficients for a multiple linear regression analysis of the %stream length that is ephemeral versus temperature (°C) and precipitation (mm) by stream order across HUC's. All coefficients had a p value of <0.01.

Stream Order	Intercept	Temp Coeff	Precip Coeff	R Square
1	93.0	2.46	-6.32E-02	0.68
2	85.1	2.89	-8.73E-02	0.87
3	69.2	2.97	-8.52E-02	0.93
4	49.5	2.92	-7.17E-02	0.87
5	30.8	2.59	-5.27E-02	0.72

Table S3. Statistics from % ephemeral days calculation. Analysis involved a multi-regression of 4,971 USGS discharge sites with a minimum of 3 years of data. The percentage of no flow days were tabulated for each site and regressed against precipitation (precip; mm) and the coefficient of variation of monthly precipitation (CV Precip) by stream order.

Stream Order	Intercept	CV Precip Coeff.	Precip Coeff.	r2
1	0.62	3.5	-4.1E-04	0.37
2	0.55	2.1	-3.5E-04	0.27
3	0.46	2.2	-3.1E-04	0.25
4	0.39	3.1	-3.1E-04	0.27
5	0.30	2.9	-2.4E-04	0.16

Table S4. Surface area, area-normalized mean gas exchange coefficient and pCO_2, and median CO_2 emission (as derived from Monte Carlo simulations) of global lakes and reservoirs, divided by area classes.

Area class (km^2)	Surface area (km^2)	Mean gas exchange coefficient *k* ($m\ d^{-1}$)	Mean pCO_2 (µatm)	Median pCO_2 emission (Pg C yr^{-1})
<0.1	211,551	0.57	1303	0.027
0.1-1	212,233	0.80	1135	0.032
1-10	370,262	0.85	966	0.048
10-100	402,597	1.09	818	0.050
>100	1,804,366	1.15	659	0.165
Sum	*3,001,009*	-	-	*0.322*

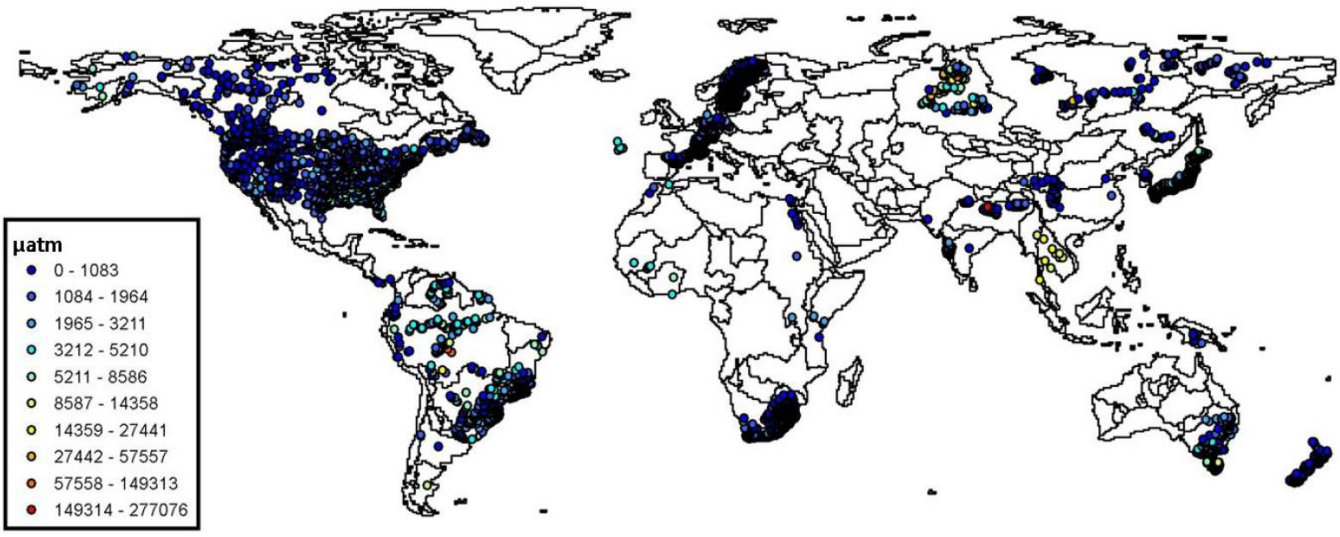

Figure 1. GLORICH River and Stream pCO_2 stations with color coded median CO_2.

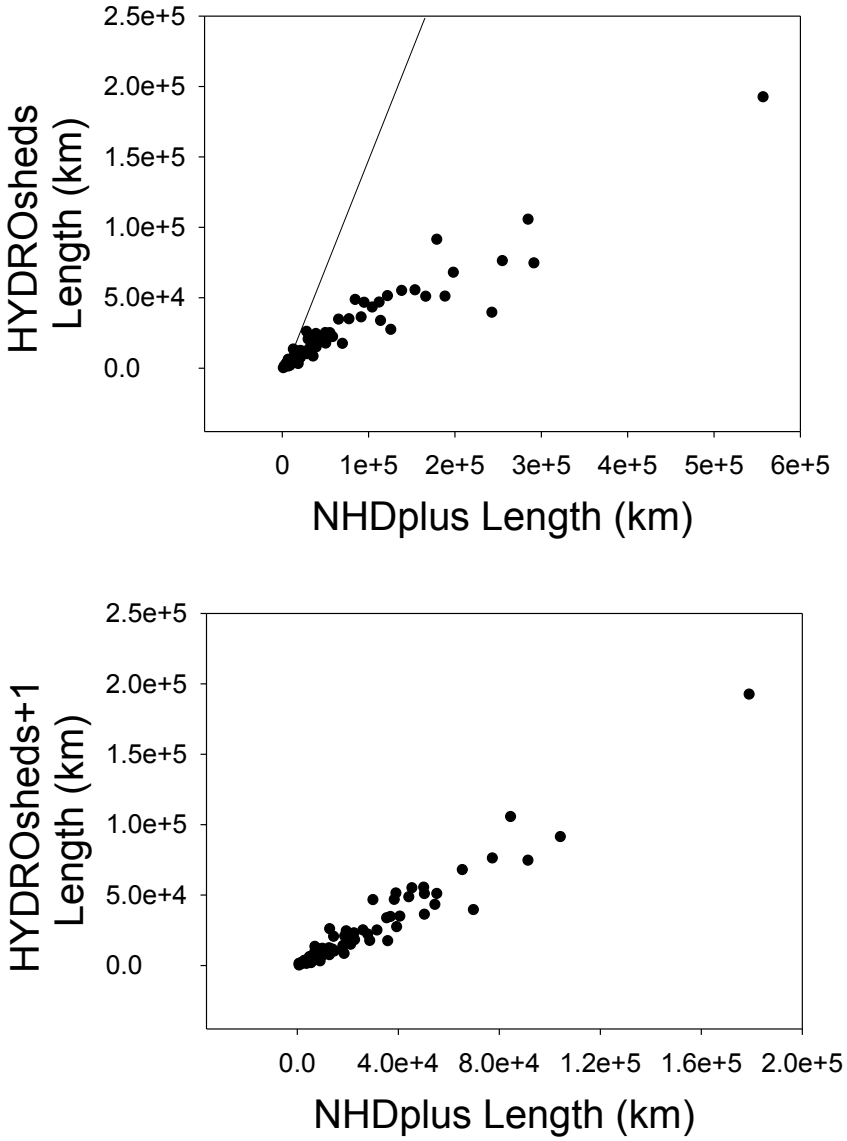

Figure 2. The relationship between stream order assignments in NHDplus and HYDROsheds for USGS HUC's stream orders 1-6. The top figure is comparing the same stream order (e.g., NHDplus stream order 1 to HYDROsheds stream order 1). The bottom figure is comparing NHDplus stream orders to the next higher HYDROshed stream order (e.g., NHDplus stream order 1 to HDROshed stream order 2). The lines are 1:1 lines.

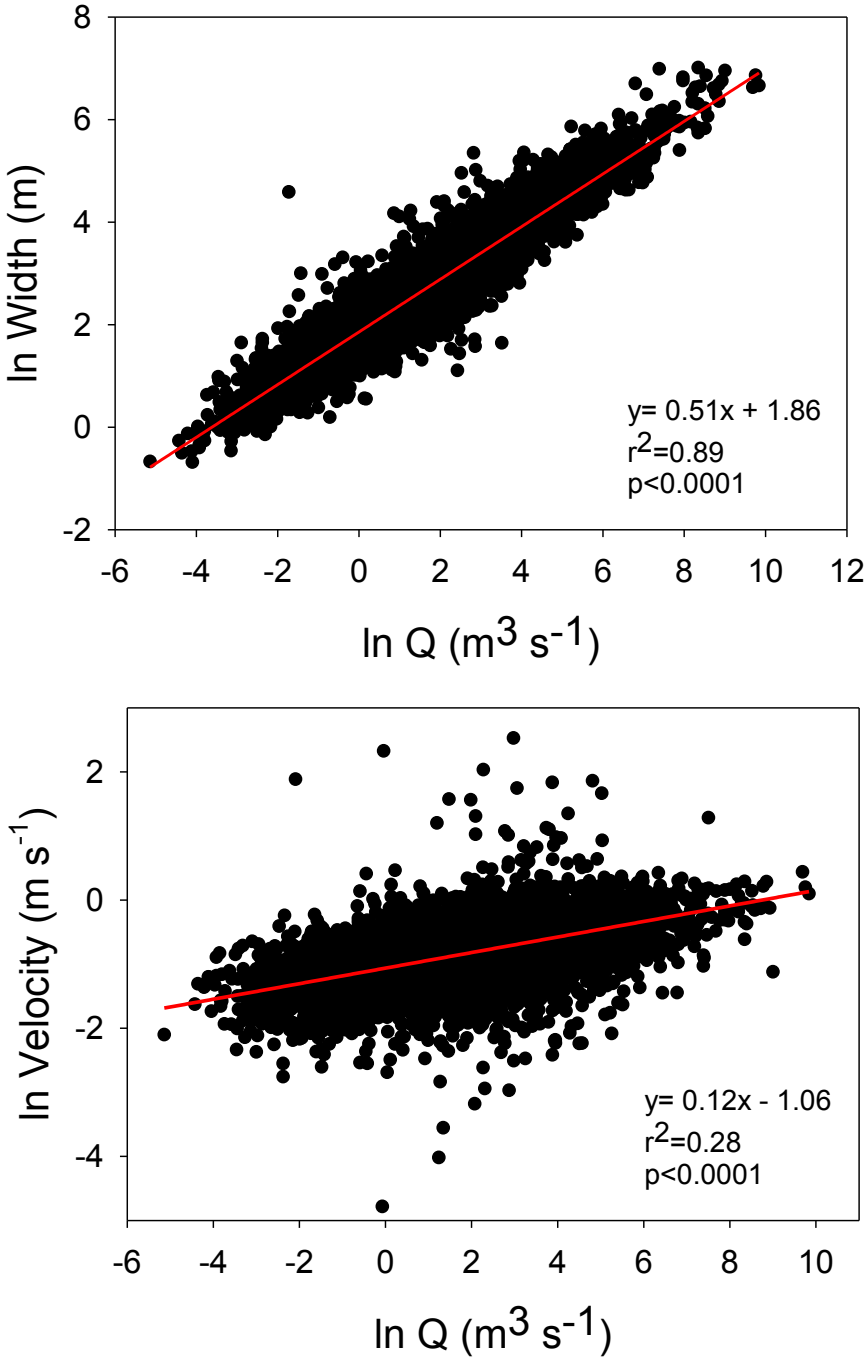

Figure 3. The hydraulic relationships for width and velocity using all available USGS gauging station data. Each data point represents one of 9811 gauging stations in the United States that had more than 20 instantaneous measurements of stream hydraulics. Data is transformed to a natural log (ln).

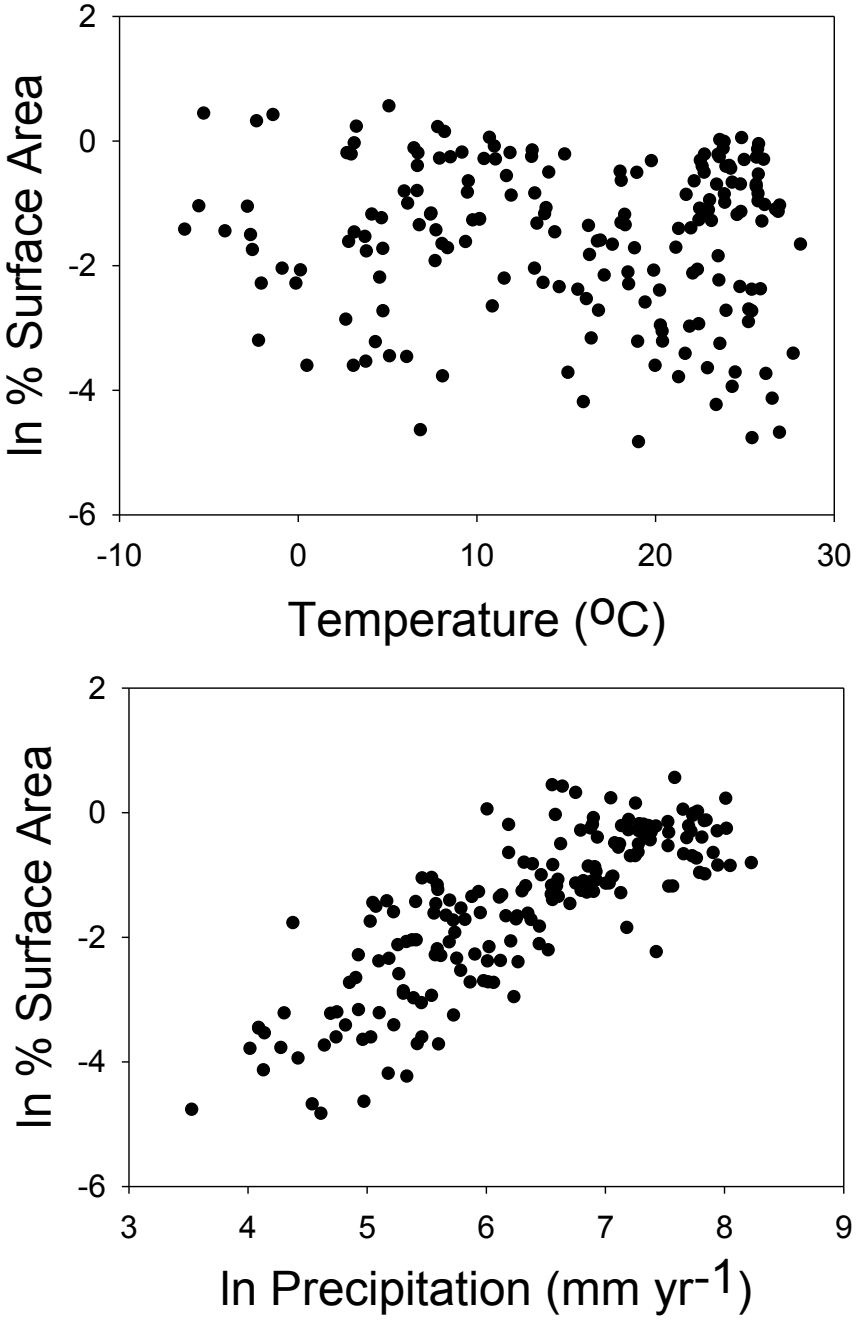

Figure 4. COSCAT temperature and precipitation versus percent surface area. Shown are the natural log of precipitation and percent surface area. Data is transformed to a natural log (ln). Data points are the average of the two equations (see text).

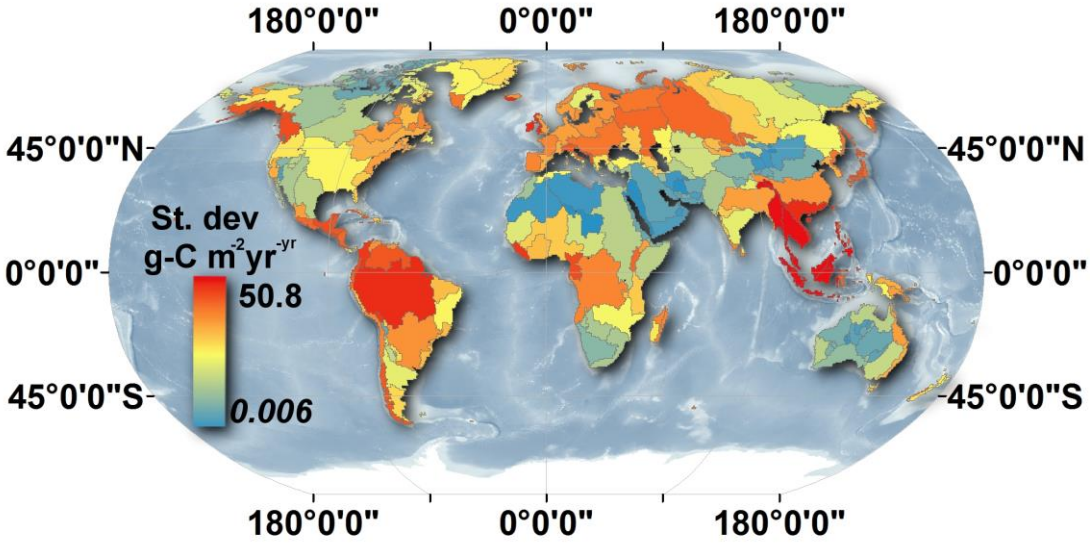

Figure 5. The standard deviation of fluxes for the stream Monte Carlo Simulation.

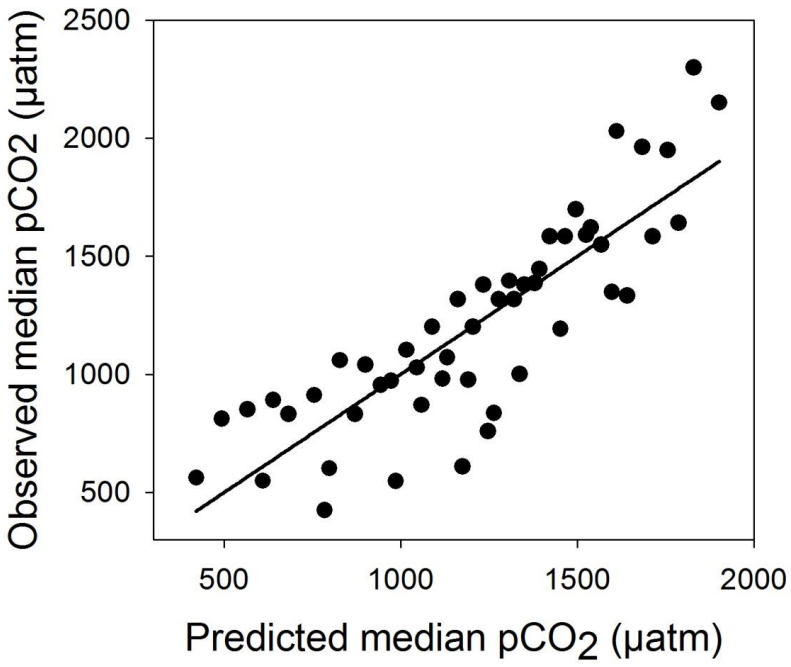

Figure 6. Median pCO_2 predicted from binned lake area and binned DOC concentration against observed values. For regression statistics, see text.

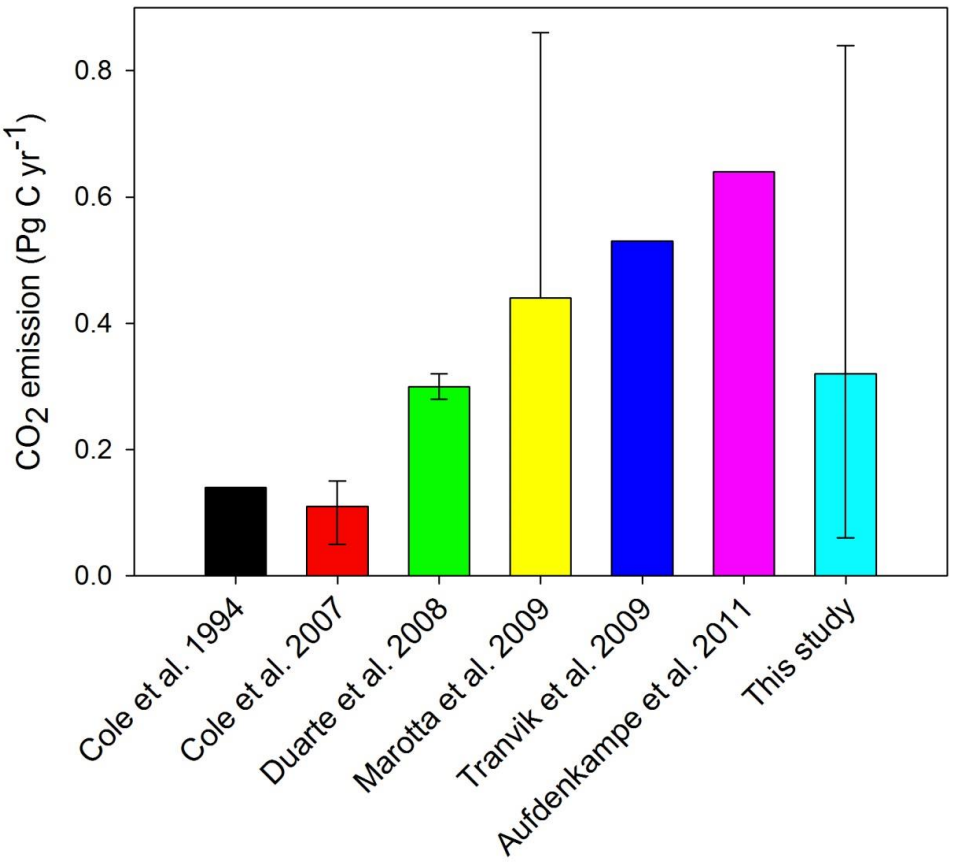

Figure 7. Comparison of published estimates of CO_2 emission from global lakes (Aufdenkampe 2011 includes reservoirs).

Works Cited

51 Parkhurst, D. L. & Appelo, C. A. J. User's guide to PHREEQC (V2)- A computer program for speciation, batch-reaction, one dimensional transport, and inverse geochemical calculations. (Denver Colorado, 1999).

52 Danielson, J. J. & Gesch, D. B. Global multi-resolution terrain elevation data 2010 (GMTED2010). 26 (2011).

53 Hartman, J., Lauerwald, R., Moosdorf, N., Amann, T. & Weiss, A. GLORICH: GLobal RIver and estuary CHemical database. *American Society of Limnology and Oceanography Meeting Abstracts* **2011** (2011).

54 Raymond, P. & Cole, J. Increased alkalinity in the Mississippi - Response. *Science* **302**, 986-987 (2003).

55 Hunt, C. W., Salisbury, J. E. & Vandemark, D. Contribution of non-carbonate anions to total alkalinity and overestimation of pCO(2) in New England and New Brunswick rivers. *Biogeosciences* **8**, 3069-3076, doi:10.5194/bg-8-3069-2011 (2011).

56 Benstead, J. P. & Leigh, D. S. An expanded role for river networks. *Nat. Geosci.* **5**, 678-679 (2012).

57 Dodds, P. S. & Rothman, D. H. Unified view of scaling laws for river networks. *Physical Review E* **59**, 4865-4877, doi:10.1103/PhysRevE.59.4865 (1999).

58 Horton, R. E. Erosional development of streams and their drainage basins- hydrophysical approach to quantitative morphology. *Geological Society of America Bulletin* **56**, 275-370 (1945).

59 Mayorga, E. *et al.* Global Nutrient Export from WaterSheds 2 (NEWS 2): Model development and implementation. *Environmental Modelling & Software* **25**, 837-853, doi:10.1016/j.envsoft.2010.01.007 (2010).

60 Guth, P. L. Drainage basin morphometry: a global snapshot from the shuttle radar topography mission. *Hydrol. Earth Syst. Sci.* **15**, 2091-2099 (2011).

61 Dodds, P. S. & Rothman, D. H. Scaling, universality, and geomorphology. *Annu. Rev. Earth Planet. Sci.* **28**, 571-610, doi:10.1146/annurev.earth.28.1.571 (2000).

62 Marotta, H., Duarte, C. M., Sobek, S. & Enrich-Prast, A. Large CO2 disequilibria in tropical lakes. *Global Biogeochemical Cycles* **23**, doi:10.1029/2008gb003434 (2009).

63 Rantakari, M. & Kortelainen, P. Interannual variation and climatic regulation of the CO2 emission from large boreal lakes. *Global Change Biology* **11**, 1368-1380, doi:10.1111/j.1365-2486.2005.00982.x (2005).

64 Sobek, S., Tranvik, L. J. & Cole, J. J. Temperature independence of carbon dioxide supersaturation in global lakes. *Global Biogeochemical Cycles* **19**, doi:Gb2003 10.1029/2004gb002264 (2005).

65 Sobek, S., Tranvik, L. J., Prairie, Y. T., Kortelainen, P. & Cole, J. J. Patterns and regulation of dissolved organic carbon: An analysis of 7,500 widely distributed lakes. *Limnol. Oceanogr.* **52**, 1208-1219 (2007).

66 Bergstrom, A. K., Algesten, G., Sobek, S., Tranvik, L. & Jansson, M. Emission of CO2 from hydroelectric reservoirs in northern Sweden. *Archiv Fur Hydrobiologie* **159**, 25-42, doi:10.1127/0003-9136/2004/0159-0025 (2004).

67 Roland, F. *et al.* Variability of carbon dioxide flux from tropical (Cerrado) hydroelectric reservoirs. *Aquatic Sciences* **72**, 283-293, doi:10.1007/s00027-010-0140-0 (2010).

68 Lozovik, P. A. Contribution of organic acid anions to the alkalinity of natural humic water. *Journal of Analytical Chemistry* **60**, 1000-1004, doi:10.1007/s10809-005-0226-3 (2005).

69 Temnerud, J. *et al.* Landscape scale patterns in the character of natural organic matter in a Swedish boreal stream network. *Hydrology and Earth System Sciences* **13**, 1567-1582 (2009).

70 Cole, J. J. & Caraco, N. F. Atmospheric exchange of carbon dioxide in a low-wind oligotrophic lake measured by the addition of SF6. *Limnol. Oceanogr.* **43**, 647-656 (1998).

71 Jonsson, A., Aberg, J., Lindroth, A. & Jansson, M. Gas transfer rate and CO(2) flux between an unproductive lake and the atmosphere in northern Sweden. *Journal of Geophysical Research-Biogeosciences* **113**, doi:10.1029/2008jg000688 (2008).

72 MacIntyre, S. *et al.* Buoyancy flux, turbulence, and the gas transfer coefficient in a stratified lake. *Geophysical Research Letters* **37**, doi:10.1029/2010gl044164 (2010).

73 Wanninkhof, R. Relationship between wind-speed and gas exchange over the ocean. *Journal of Geophysical Research-Oceans* **97**, 7373-7382, doi:10.1029/92jc00188 (1992).

74 Jahne, B. *et al.* On the parameters influencing air-water gas exchange. *Journal of Geophysical Research-Oceans* **92**, 1937-1949, doi:10.1029/JC092iC02p01937 (1987).

75 Striegl, R. G. *et al.* Carbon dioxide partial pressure and C-13 content of north temperate and boreal lakes at spring ice melt. *Limnol. Oceanogr.* **46**, 941-945 (2001).